



# Weakened SST variability in the tropical Atlantic Ocean since 2000

Arthur Prigent<sup>1</sup> · Joke F. Lübbecke<sup>1,2</sup> · Tobias Bayr<sup>1</sup> · Mojib Latif<sup>1,2</sup> · Christian Wengel<sup>3</sup>

Received: 2 July 2019 / Accepted: 14 January 2020 / Published online: 27 January 2020  
© Springer-Verlag GmbH Germany, part of Springer Nature 2020

## Abstract

A prominent weakening in equatorial Atlantic sea surface temperature (SST) variability, occurring around the year 2000, is investigated by means of observations, reanalysis products and the linear recharge oscillator (ReOsc) model. Compared to the time period 1982–1999, during 2000–2017 the May–June–July SST variability in the eastern equatorial Atlantic has decreased by more than 30%. Coupled air–sea feedbacks, namely the positive Bjerknes feedback and the negative net heat flux damping are important drivers for the equatorial Atlantic interannual SST variability. We find that the Bjerknes feedback weakened after 2000 while the net heat flux damping increased. The weakening of the Bjerknes feedback does not appear to be fully explainable by changes in the mean state of the tropical Atlantic. The increased net heat flux damping is related to an enhanced response of the latent heat flux to the SST anomalies (SSTa). Strengthened trade winds as well as warmer SSTs are suggested to increase the air–sea specific humidity difference and hence, enhancing the latent heat flux response to SSTa. A combined effect of those two processes is proposed to be responsible for the weakened SST variability in the eastern equatorial Atlantic. The ReOsc model supports the link between reduced SST variability, weaker Bjerknes feedback and stronger net heat flux damping.

**Keywords** Atlantic Niño · Ocean and atmosphere dynamics · Bjerknes feedback · Net heat flux damping

## 1 Introduction

The equatorial Atlantic Ocean is characterized by interannual variations of sea surface temperature (SST), which can have significant impacts on the climate over the adjacent landmasses (Hirst and Hastenrath 1983; Folland et al. 1986; Nobre and Shukla 1996). The dominant mode of tropical Atlantic interannual SST variability, which has its center of action in the equatorial cold tongue region, is referred to as the Atlantic Niño or Atlantic zonal mode because of its east–west orientation (see Lübbecke et al. (2018) for a review). The underlying dynamics of the Atlantic Niño are to some extent similar to those observed during El Niño/Southern Oscillation (ENSO) in the Pacific Ocean (Servain

et al. 1982; Zebiak 1993; Keenlyside and Latif 2007). They involve a coupling of SST anomalies (SSTa), zonal wind stress and ocean heat content anomalies as described by the Bjerknes feedback (Bjerknes 1969). The Atlantic Niño exhibits a clear seasonal phase locking with largest SSTa occurring in boreal summer (Richter et al. 2017) and a secondary maximum peaking in November–December referred to as Atlantic Niño II by Okumura and Xie (2006). While the Atlantic Niño shares many characteristics with ENSO, it is more damped (Zebiak 1993; Lübbecke and McPhaden 2013), and the events are of shorter duration than for the Pacific counterpart. Compared to ENSO, each of the three Bjerknes feedback components, i.e. (1) the zonal wind response to eastern equatorial SSTa, (2) the thermocline slope response to western equatorial wind anomalies and (3) the local response of SSTa to thermocline depth anomalies, explains less variance in the tropical Atlantic (Keenlyside and Latif 2007), allowing other processes to play an important role as well. Nnamchi et al. (2015) showed that thermodynamic forcing by stochastic atmospheric perturbations can explain a significant amount of the observed SST variability in the equatorial Atlantic. Yet, recent studies assessing the relative importance of dynamic versus thermodynamic

✉ Arthur Prigent  
aprigent@geomar.de

<sup>1</sup> GEOMAR Helmholtz Centre for Ocean Research Kiel, Kiel, Germany

<sup>2</sup> Faculty of Mathematics and Natural Sciences, Christian Albrechts University, Kiel, Germany

<sup>3</sup> Center for Climate Physics, Institute for Basic Science, Busan, South Korea

processes conclude that the dynamic and in particular the Bjerknes feedback is a main driver for the Atlantic zonal mode (Jouanno et al. 2017; Dippe et al. 2019).

Some studies have addressed multidecadal change of SST variability both in the equatorial Pacific (Hu et al. 2013; Lübbecke and McPhaden 2014; Guan and McPhaden 2016; Hu et al. 2017; Xu et al. 2019) and in the equatorial Atlantic (Tokinaga and Xie 2011). While Tokinaga and Xie (2011) investigated trends in Atlantic cold tongue variability over the time period 1950–2009, several studies have discussed a shift in equatorial Pacific variability that occurred around the year 2000 and is clearly visible in many ENSO characteristics. This shift has been explained by changes in the equatorial thermocline tilt along with a strengthening of the trade winds, which has hampered the eastward migration of warm water along the equatorial Pacific and hence reduced ENSO amplitude (Hu et al. 2013). A more recent study from Xu et al. (2019), also investigating the weakening of ENSO amplitude since the late 1990s, put it in the context of the transition from the Aleutian Low mode to the North Pacific Oscillation in the atmosphere that is responsible for a westward extension of negative sea level pressure anomalies. This shift is proposed to have weakened the atmospheric responses to the zonal equatorial SSTa, and hence ENSO amplitude.

In the present study, we want to investigate a shift in SST variability in the eastern equatorial Atlantic that has occurred around the year 2000. The paper is structured as follows: The data and methods used are described in Sect. 2. In Sect. 3, the shift in interannual SST variability and mean state changes are investigated. Summary and discussion are presented in Sect. 4.

## 2 Data and methods

### 2.1 Data

#### 2.1.1 Ocean variables, wind and precipitation datasets

Nine reanalysis and observational datasets with monthly resolution are used for SST over the time period 1982–2017. The analyzed datasets are: the Hadley Centre Sea Ice and Sea Surface Temperature dataset version 1.1 (HadI-SST 1.1, Rayner (2003), which is an EOF-based reconstruction, available at 1° by 1° horizontal resolution and spanning the period 1870/01–2018/12; The Ocean Reanalysis System version 4 (ORA-S4, Balmaseda et al. 2013) from the European Centre for Medium-range Weather Forecast (ECMWF) available at 1° by 1° horizontal resolution for the time period 1958/01 to 2017/12; the Optimum Interpolation SST Analysis Version 2 (OI-SST, Reynolds et al. 2007) available at 1° by 1° horizontal resolution for the time period 1981/12 to

2019/05; the Climate Forecast System Reanalysis Version 1 and 2 (CFSR, Saha et al. 2014) available at 2.5° by 2.5° horizontal resolution for the time period 1979/01 to 2019/08; The ECMWF Re-Analysis 5 (ERA5) product (Hersbach and Dee 2016) available at 0.5° by 0.5° horizontal resolution for the time period 1979/01 to 2019/06; The ECMWF Re-Analysis (ERA)-interim product (Dee et al. 2011) available at 0.5° by 0.5° horizontal resolution for the time period 1979/01–2018/12; the Woods Hole Oceanographic Institution Objectively Analyzed air sea Fluxes (OAflux; Yu et al. 2008) and National Centers for Environmental Prediction/ National center for Atmospheric Research (NCEP/NCAR) Reanalysis 1 (NCEP-R1, Kalnay et al. 1996) and NCEP/DOE Reanalysis 2 (NCEP-R2, Kanamitsu et al. 2002) available at 2.5° by 2.5° horizontal resolution spanning the time periods from 1979/01 to 2018/12 for OAflux and NCEP-R2 and from 1948/01 to 2019/05 for NCEP-R1.

Ocean subsurface temperature data to calculate the depth of the 23 °C isotherm as a proxy for thermocline depth (Lübbecke and McPhaden 2013) is taken from the ORA-S4 reanalysis dataset. Wind speed and wind stress data spanning the time period 1982–2017 are taken from ERA-interim, ERA5, CFSR, NCEP-R1, and NCEP-R2. Monthly precipitation data is taken from the Global Precipitation Climatology Project version 2.3 (GPCP, Adler et al. 2018), which is a blend of satellite and station data, available at 2.5° by 2.5° horizontal resolution for the time period 1979/01–2019/04.

Reanalysis datasets are known to have large biases in the tropical regions (Kumar and Hu 2012) and particularly in the tropical Atlantic Ocean (Huang et al. 2007). These biases may have an impact on the ocean–atmosphere feedbacks and overshadow the changes between the two periods. However, the use of several datasets allows us to assess the robustness of our results.

#### 2.1.2 Heat flux products

Six monthly heat flux products are used for the time period 1982–2017: OAflux, ERA-interim, NCEP-R1 and NCEP-R2, ERA5, and CFSR. Heat fluxes are estimated and based on the use of bulk formulas and thus require the knowledge of several variables such as the wind speed, specific air and surface humidity, air and surface temperatures. Significant differences can exist between the different heat flux products (Bentamy et al. 2017). We therefore use six different products to assess the robustness of our results. The net heat flux ( $Q_{\text{net}}$ ) can be decomposed into the sum of four components:

$$Q_{\text{net}} = Q_{\text{sw}} + Q_{\text{lw}} + Q_{\text{sh}} + Q_{\text{lh}}, \quad (1)$$

where  $Q_{\text{sw}}$  is the shortwave radiation flux,  $Q_{\text{lw}}$  is the long-wave radiation flux, and  $Q_{\text{sh}}$  and  $Q_{\text{lh}}$  are the turbulent

sensible and latent heat flux, respectively. The latent heat flux can be estimated with the bulk formula (Bentamy et al. 2003):

$$Q_{lh} = L \times \rho_{air} \times C_E \times (Q_s - Q_a) \times U_s, \quad (2)$$

$$L = 4186.8 \times (597.31 - 0.5625T_s), \quad (3)$$

$L$  is the latent heat of vaporization with a typical value of  $2.5 \times 10^6$  J/kg,  $Q_a$  is the near-surface air specific humidity,  $U_s$  is the 10 m wind speed and  $\rho_{air}$  is the air density.

$$C_E = 10^{-3} a \exp[b(U_{10} + c)] + \frac{d}{U_{10}} + 1 \quad (4)$$

The Dalton number,  $C_E$  is a function of the wind speed and ranges between 0.0015 and 0.0011 for wind speeds between 2 and 20  $\text{m.s}^{-1}$ . With  $a = -0.146785$ ,  $b = -0.292400$ ,  $c = -2.206$  and  $d = 1.612292$ .  $Q_s$ , the saturated surface humidity, has been estimated using the formula:

$$Q_s = \frac{5}{8} \frac{es}{ps - es}, \quad (5)$$

where  $es = T_s^A \times 10^{B+C/T_s}$  with  $a = -4.928$ ,  $b = 23.55$  and  $c = -2937$ .

## 2.2 Methods

In order to investigate the reasons behind the weakened SST variability in the eastern equatorial Atlantic since the year 2000, the strength of the Bjerknes feedback and the net heat flux damping, are estimated for the time period 1982/01 to

1999/12 and 2000/01 to 2017/12. First, the Bjerknes feedback is estimated via linear regression analysis of (1) western equatorial Atlantic (WAtl) zonal wind stress anomalies ( $3^\circ \text{S}$ – $3^\circ \text{N}$  and  $40^\circ \text{W}$ – $20^\circ$ , Fig. 1) upon Atl3-averaged SSTa ( $3^\circ \text{S}$ – $3^\circ \text{N}$  and  $20^\circ \text{W}$ – $0^\circ$ , Fig. 1), (2) Equatorial thermocline slope anomalies upon WAtl zonal wind stress anomalies and (3) SSTa upon thermocline depth anomalies pointwise in the Atl3 region. The equatorial thermocline slope is computed as the difference between the mean Atl3  $23^\circ \text{C}$  isotherm depth ( $Z_{23}$ ) and WAtl  $Z_{23}$ . Second, the net heat flux damping is estimated via the linear regression of net heat flux anomalies upon SSTa in the Atl3 region. Prior to the regressions the linear trend has been removed from all datasets. All analyses are based on monthly-mean anomalies computed by subtracting the climatological monthly mean seasonal cycle calculated separately for each dataset and time period. Equally long periods relative to 2000 are chosen, but taking a longer pre-2000 period does not fundamentally change the results (see Table 1).

To support the interpretation of the results the linear recharge oscillator model from Burgers et al. (2005) (hereafter referred to as ReOsc model) is used, which describes the oscillatory behavior of the equatorial Atlantic variability by the interaction of eastern equatorial Atlantic SST and equatorial mean upper ocean heat content:

$$\frac{dT}{dt} = a_{11}T + a_{12}h + \varepsilon_T, \quad (6)$$

$$\frac{dh}{dt} = a_{21}T + a_{22}h + \varepsilon_h, \quad (7)$$

**Fig. 1** Difference of ORA-S4 standard deviation of SST ( $^\circ\text{C}$ ) anomalies between 2000–2017 and 1982–1999. Three regions used in the following are indicated by boxes: the Atlantic 3 region (Atl3;  $3^\circ \text{S}$ – $3^\circ \text{N}$ ,  $20^\circ \text{W}$ – $0^\circ$ ) in green, the western Atlantic region (WAtl;  $3^\circ \text{S}$ – $3^\circ \text{N}$ ,  $40^\circ \text{W}$ – $20^\circ$ ) in red and the Equatorial Atlantic region (EqAtl;  $5^\circ \text{S}$ – $5^\circ \text{N}$ ,  $50^\circ \text{W}$ – $20^\circ \text{E}$ ) in blue. Dots represent where standard deviation of the SSTa of the two periods are significantly different at the 95%-level according to the Welch's  $t$  test

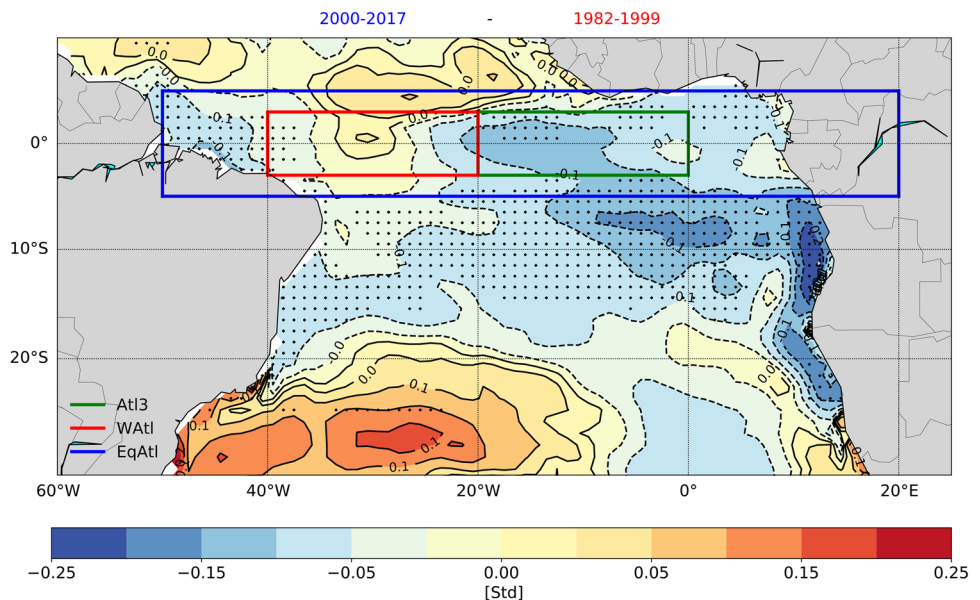


**Table 1** Standard deviation of MJJ (NDJ) SST anomalies averaged over the Atl3 region during 1982–1999 and 2000–2017

Product	1960–1999	1982–1999	2000–2017	Reduction (%)
OI-SST	–	0.76 (0.49)	0.54 (0.47)	29 (4.1)
ORA-S4	0.67 (0.50)	0.73 (0.47)	0.52 (0.42)	29 (10.6)
Hadl-SST	0.66 (0.50)	0.50 (0.46)	0.34 (0.35)	31 (22.2)
CFSR	–	0.59 (0.43)	0.45 (0.41)	24 (4.6)
ERA5	–	0.72 (0.51)	0.47 (0.42)	35 (17.6)
ERA-interim	–	0.67 (0.44)	0.48 (0.39)	28 (11.3)
OAflux	–	0.65 (0.42)	0.45 (0.38)	32 (9.5)
NCEP-R1	0.67 (0.55)	0.77 (0.42)	0.48 (0.42)	38 (6.6)
NCEP-R2	–	0.76 (0.45)	0.48 (0.42)	37 (6.6)
EM	0.67 ± 0.005 (0.52 ± 0.02)	0.68 ± 0.09 (0.45 ± 0.03)	0.47 ± 0.05 (0.41 ± 0.03)	31 (9)

The reduction is relative to the first period. EM is the ensemble mean of the SST products

where  $T$  is the Atl3 SSTa and  $h$  is the mean thermocline depth anomalies averaged over the Equatorial Atlantic region ( $5^\circ \text{S}$ – $5^\circ \text{N}$ ,  $50^\circ \text{W}$ – $20^\circ \text{E}$ , EqAtl, Fig. 1). The parameters  $a_{11}$  and  $a_{22}$  represent the damping (or growth rate) of  $T$  and  $h$ , respectively.  $a_{12}$  and  $a_{21}$  are the coupling of  $T$  to  $h$  and  $h$  to  $T$ , respectively. The tendency equation of  $T$  and  $h$  are forced by the stochastic noise of  $T$  and  $h$ ,  $\varepsilon_T$  and  $\varepsilon_h$ , evaluated as the standard deviation of the residual of the linear regression fit, which can be interpreted as a random noise forcing. It is noted that in this framework, the stochastic forcing terms may contain also nonlinear contributions which still are dependent on the prognostic variables  $T$  and  $h$ . As this study is focusing on the oceanic and atmospheric processes contributing to the weakened SST variability, the coefficient  $a_{11}$  is further decomposed into its oceanic and atmospheric part (Frauen and Dommenges 2010):

$$a_{11} = a_{11O} + a_{11A}, \quad (8)$$

$$a_{11A} = \underbrace{a_{12}\lambda C_{\tau T}}_{a_{11\text{wind}}} + \underbrace{\frac{C_{ft}}{\gamma}}_{a_{11\text{HF}}}, \quad (9)$$

where  $C_{\tau T}$  is the wind stress (Bjerknes) feedback estimated by the linear regression of zonal wind stress in the WAtl box (Fig. 1) onto  $T$ .  $C_{ft}$  is the heat flux feedback evaluated as the linear regression of the net atmospheric flux upon  $T$  in the Atl3 region.  $\lambda$  and  $\gamma$  are the positive coupling parameter and the scaled ocean mixed-layer depth, which are assumed to be constant and amount to  $2100 \text{ m}^3 \text{ N}^{-1}$  and  $48.9 \text{ K m}^2 \text{ W}^{-1} \text{ month}$ , respectively.  $a_{11O}$  is the residual of  $a_{11}$  when  $a_{11A}$  is estimated as in Eq. 9, it is expected to be driven by oceanic feedbacks such as the dynamical damping from mean ocean currents and the zonal advective feedback, Ekman feedback and the thermocline feedback as inferred from oceanic contributions in the Bjerknes Stability Index analysis (Jin et al. 2006).

Finally, following the approach of Bayr et al. (2014) we compute the zonal streamfunction:

$$\psi = 2\pi a \int_0^p u_D \frac{dp}{g}, \quad (10)$$

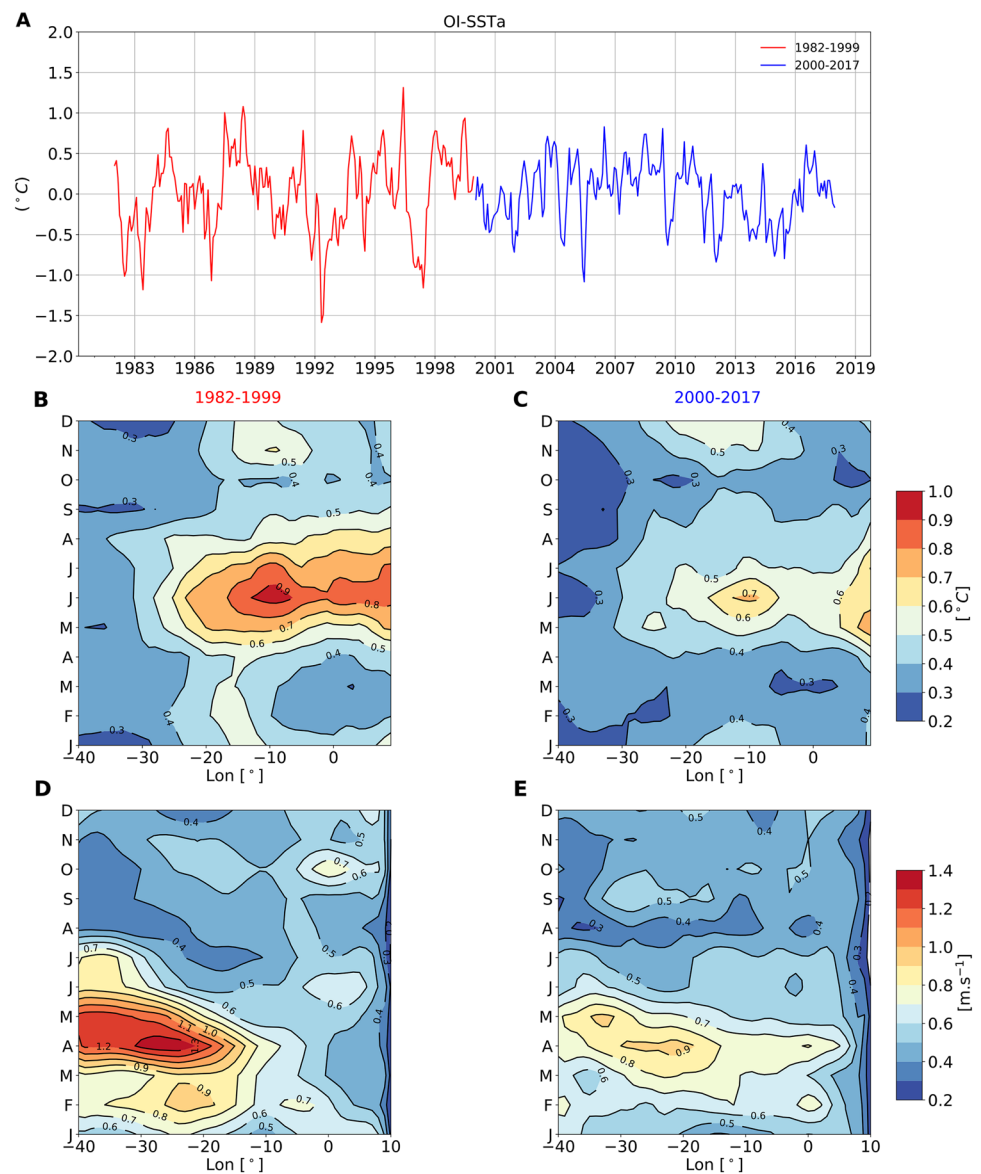
where  $u_D$  is the divergent component of the zonal wind,  $a$  is the radius of the earth,  $p$  the pressure and  $g$  the gravity constant. The zonal wind is averaged between  $3^\circ \text{N}$  and  $3^\circ \text{S}$  and integrated from the top of the atmosphere to surface.

### 3 Results

#### 3.1 Observed changes in interannual variability

Interannual SST variability in the eastern equatorial Atlantic featured a strong change in magnitude around the year 2000 (Figs. 1, 2a). The averaged May–June–July (MJJ) SST standard deviation in the Atl3 region ( $3^\circ \text{S}$ – $3^\circ \text{N}$ ,  $20^\circ \text{W}$ – $0^\circ$ , Fig. 1) during 1982–1999 was  $0.68 \pm 0.09 \text{ K}$  as derived from the ensemble mean of the nine SST products (Table 1), whereas the variability decreased by 31% to  $0.47 \pm 0.05 \text{ K}$  during 2000–2017. In contrast, the averaged November–December–January (NDJ) SST standard deviation in the Atl3 region shows only small changes from  $0.45 \pm 0.03 \text{ K}$  during 1982–1999 to  $0.41 \pm 0.03 \text{ K}$  during 2000–2017. The seasonal evolution of the SST standard deviation along the equator during 1982–1999 depicts a distinct yearly maximum in boreal summer (Fig. 2b), which is consistent with the seasonally shoaling thermocline depth and maximum surface–subsurface coupling (Keenlyside and Latif 2007; Harlaß et al. 2015). In November–December (ND), there is a secondary maximum of SST variability, consistent with the findings of Okumura and Xie (2006). The strengthening easterly winds in ND raise the thermocline in the Gulf

**Fig. 2** **a** Time series of OI-SST anomalies averaged over the Atl3 region ( $3^{\circ}\text{S}$ – $3^{\circ}\text{N}$ ,  $20^{\circ}\text{W}$ – $0^{\circ}$ ) during 1982–1999 (red) and 2000–2017 (blue). **b, c** Standard deviation of OI-SSTa along the equator and averaged between  $3^{\circ}\text{S}$  and  $3^{\circ}\text{N}$  for the period 1982–1999 and 2000–2017, respectively. **d, e** Standard deviation of ERA-interim zonal wind speed anomalies along the equator averaged between  $3^{\circ}\text{S}$  and  $3^{\circ}\text{N}$  for the period 1982–1999 and 2000–2017, respectively



of Guinea, which reactivates the Bjerknes feedback during this short period. After 2000, the same seasonal pattern of SST variability is observed but with overall reduced variability (Fig. 2c). Figure 2d depicts a maximum of zonal wind variability in April–May–June (AMJ) in the western equatorial Atlantic basin, as measured by the standard deviation of the zonal wind speed anomalies. During 1982–1999, the AMJ WAtl zonal wind speed variability, derived as the ensemble mean of the wind products (Table 2), amounts to  $0.89 \pm 0.11 \text{ m s}^{-1}$ , whereas in 2000–2017 the variability decreased to a value of  $0.76 \pm 0.09 \text{ m s}^{-1}$ . The reduction of the AMJ WAtl wind variability is consistent among the datasets, only NCEP-R1 and NCEP-R2 show a smaller reduction.

**Table 2** Standard deviation of AMJ zonal wind speed anomalies at 10 meters averaged over the WAtl region during 1982–1999 and 2000–2017

Wind product	1982–1999	2000–2017	Reduction (%)
ERA-interim	1.04	0.74	28.8
ERA5	0.98	0.78	20.4
CFRS	0.71	0.61	14.1
NCEP-R1	0.84	0.82	2.0
NCEP-R2	0.87	0.87	0.0
EM	$0.89 \pm 0.11$	$0.76 \pm 0.09$	15

The reduction is relative to the first period. EM is the ensemble mean of the wind products



### 3.2 Weakened Bjerknes feedback

The Atlantic Niño mode is in part determined by ENSO-like dynamics (Servain et al. 1982; Keenlyside and Latif 2007; Deppenmeier et al. 2016; Lübbecke and McPhaden 2017), in particular by the Bjerknes feedback which can be decomposed into its three components: (1) the zonal wind response to eastern equatorial SSTa, (2) the thermocline slope response to western equatorial wind anomalies and (3) the local response of SSTa to thermocline depth anomalies. In order to understand the pronounced weakening in the SST variability in MJJ after the year 2000 we first calculate the individual components of the Bjerknes feedback separately for the two time periods 1982–1999 and 2000–2017. As the Bjerknes feedback is strongly seasonal, the three components of the Bjerknes feedback are first estimated as a function of the calendar month (Fig. 3) and then averaged for the relevant seasons (Fig. 4) via linear regression for the two time periods. The first component is peaking in AMJ (Fig. 3a) while the second and third components are peaking in MJJ. From Figs. 2 and 3 we decide to focus on MJJ and NDJ when the Bjerknes feedback and interannual SST variability are the highest.

First, the western zonal wind stress response to eastern equatorial Atlantic SSTa is investigated (Fig. 4a, d). Relative to the time period 1982–1999, after 2000 the zonal wind stress response to Atl3 SSTa has weakened by 21% in MJJ and by 24.5% in NDJ. The second component (Fig. 4b, e), i.e. the thermocline slope response to western equatorial zonal wind stress anomalies which is driven by the eastward propagation of equatorial Kelvin waves, has also weakened. Compared to 1982–1999, after 2000 the second component has reduced by 30.2% in MJJ and by 32.7% in NDJ (Fig. 4b, e). The third component, i.e. the local response of SSTa to

changes in thermocline depth has not experienced any significant change. We note the smaller amount of variance accounted for by the three components since 2000, suggesting that the Bjerknes feedback has become a less important driver of SST variability in the equatorial Atlantic. The same linear regression analysis has also been performed using different products and months. We find that while the regressions are sensitive to the chosen period, the overall general result, i.e. a weakening of the Bjerknes feedback strength, remains the same.

### 3.3 Net heat flux damping

Thermodynamical processes are also known to play an important role in the equatorial Atlantic variability. While their damping effect has been long recognized (e.g. Frankignoul et al. 2002), they have also been suggested to contribute to the onset of Atlantic Niño events (Nnamchi et al. 2015). The ocean and the atmosphere are coupled through heat fluxes. The turbulent heat exchange, i.e. the latent and sensible heat fluxes, allow the ocean to release the heat absorbed from solar radiation. This heat release is responsible for damping the SSTa and hence reducing its variability. The net heat flux damping is the dominant negative feedback in the equatorial Atlantic (Lübbecke and McPhaden 2013). It is estimated via linear regression of net heat flux anomalies upon SSTa. We use six different heat flux products to get a sense of the uncertainty.

Relative to 1982–1999, in 2000–2017 we observe a stronger MJJ net heat flux damping (Table 3) with an increase from  $-16.52 \pm 4.59$  to  $-23.96 \pm 5.92 \text{ W m}^{-2} \text{ K}^{-1}$  and from  $-8.93 \pm 7.44$  to  $-14.57 \pm 8.07 \text{ W m}^{-2} \text{ K}^{-1}$  in NDJ as derived from the ensemble mean of the heat flux products.

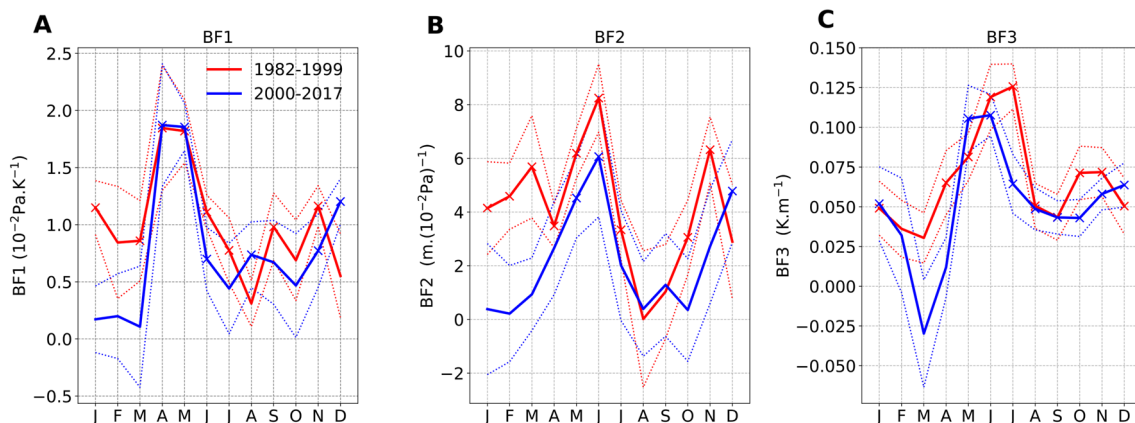


**Fig. 3** Bjerknes feedback components as a function of the calendar months for the period 1982–1999 (red) and 2000–2017 (blue). **a** Zonal wind response to eastern equatorial SST changes. **b** Thermocline slope response to western equatorial surface wind anomalies.

**c** Local response of SSTa to thermocline depth anomalies. Crosses indicate that the regressions are significant at the 95%-level according to the Student's *t* test. Dotted lines depict the error bars of the regressions

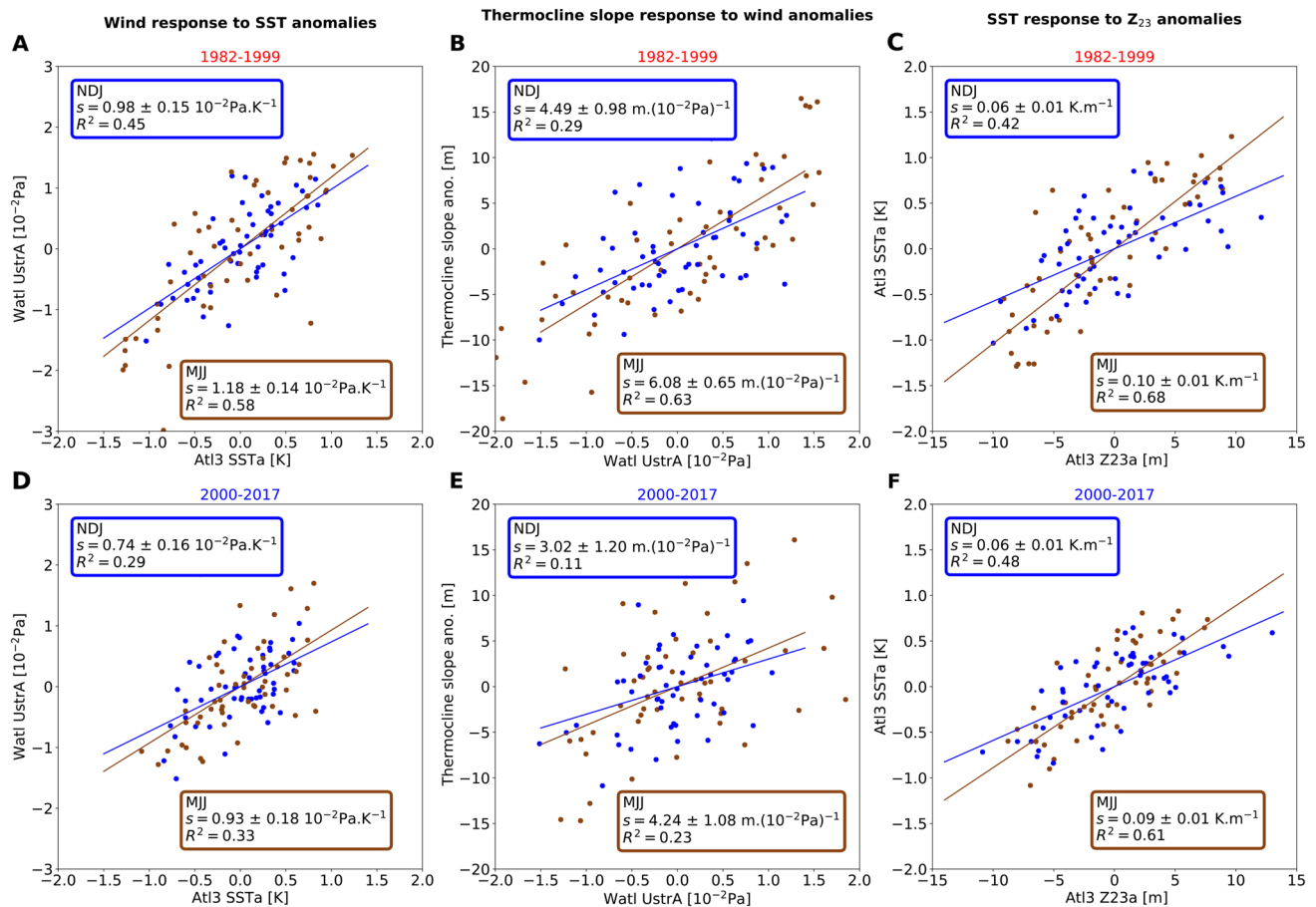


**Fig. 4** Bjerknes feedback components for the equatorial Atlantic for 1982–1999 (upper row) and for 2000–2017 (lower row). **a, d** Linear regression of MJJ AtI3 SST upon MJJ western equatorial Atlantic zonal wind stress anomalies (Watl, brown) and of November–December–January (NDJ) AtI3 SST upon NDJ Watl wind stress anomalies (dark blue). Linear regression of MJJ (NDJ) Watl wind

anomalies upon MJJ (NDJ) equatorial thermocline slope anomalies (brown and dark blue: **b** and **e**, respectively). Linear regression of MJJ (NDJ) AtI3  $Z_{23}$  anomalies upon MJJ (NDJ) SST anomalies (brown and dark blue: **c** and **f**, respectively). Regressions are significant at 95% according to the Student's  $t$  test.  $S$  is the slope of the regression line and  $R^2$  is the correlation coefficient squared

**Table 3** MJJ AtI3 net heat flux damping (latent heat flux damping) during the periods 1982–1999 and 2000–2017

Product	1982–1999		2000–2017	
	MJJ	NDJ	MJJ	NDJ
CFSR	−13.43 (−16.17)	1.45 (−8.21)	−16.02 (−17.75)	−2.01 (−8.18)
ERA5	−18.24 (−15.98)	−14.1 (−11.03)	−24.15 (−21.42)	−13.76 (−8.95)
ERA-interim	−16.95 (−12.61)	−16.21 (−6.38)	−23.15 (−17.35)	−22.44 (−12.24)
OAflux	−10.43 (−11.84)	−9.34 (−8.78)	−19.08 (−17.88)	−23.30 (−12.66)
NCEP-R1	−14.96 (−8.86)	−16.1 (−9.27)	−26.68 (−19.89)	−19.61 (−13.1)
NCEP-R2	−25.12 (−16.76)	0.7 (−5.18)	−34.69 (−30.79)	−6.29 (−12.67)
EM	−16.52 ± 4.59 (−13.70 ± 2.85)	−8.93 ± 7.44 (−8.14 ± 1.91)	−23.96 ± 5.92 (−20.85 ± 4.67)	−14.57 ± 8.07 (−11.30 ± 1.96)

EM is the ensemble mean of the heat flux products

We decompose the net heat flux into its different components and look separately at the response of each component to the SSTa. The latent heat flux response to SSTa is found to be the most important component with an increase from

−13.70 ± 2.85 to −20.85 ± 4.67 W m<sup>−2</sup> K<sup>−1</sup> in MJJ and from −8.14 ± 1.91 to −11.30 ± 1.96 W m<sup>−2</sup> K<sup>−1</sup> in NDJ. The sensible heat flux damping has also increased but is smaller in total numbers (not shown). The stronger net heat

**Table 4** MJJ near-surface specific humidity difference response to Atl3 SST changes for the periods 1982–1999 and 2000–2017

Product	1982–1999	2000–2017
CFSR	0.50	0.56
ERA5	0.82	0.93
ERA-interim	–	–
OAflux	0.59	0.71
NCEP-R1	0.70	0.76
NCEP-R2	0.59	0.82
EM	$0.64 \pm 0.11$	$0.76 \pm 0.12$

EM is the ensemble mean of the heat flux products

flux damping due to the latent heat flux is consistent among the datasets (Table 3).

Lloyd et al. (2011) argued that the latent heat flux damping in the equatorial Pacific is mainly driven by near-surface specific humidity difference whereas the winds play only a secondary role. Calculating both the response of the Atl3 zonal wind and the Atl3 near-surface specific humidity difference to Atl3 SSTa, we find that only the latter showed a significant change when comparing the two time periods (Table 4), consistent with the findings by Lloyd et al. (2011) for the Pacific.

Relative to 1982–1999, in 2000–2017 the MJJ Atl3 near-surface specific humidity difference response to SSTa increased (Table 4) from  $0.64 \pm 0.11$  to  $0.76 \pm 0.12$  g kg<sup>-1</sup> K<sup>-1</sup>. This suggests that the increase in latent heat flux damping is mainly driven by the increased response of the near-surface specific humidity.

### 3.4 Mean state changes

Contemporaneously with the reduced SST variability, the tropical Atlantic mean state has also undergone changes over the past decades. We here investigate the mean state changes to see whether the changes in the Bjerknes feedback and heat flux damping can be related to them.

We observe a sustained positive trend in the SST averaged over the tropical Atlantic basin (20° S–30° N, 60° W–15° E) since 1982 (Fig. 5a). However, the MJJ SST difference (Fig. 5b) between 1982–1999 and 2000–2017 mainly depicts a significant warming of about 0.3° C north of the equator but no significant change in the eastern equatorial Atlantic. Figure 5c shows the March–April–May (MAM) wind speed difference superimposed on the precipitation difference between the two periods as well as the 5 and 10 mm day<sup>-1</sup> precipitation contours as a proxy for the position of the Inter-tropical convergence zone (ITCZ). Relative to 1982–1999, in 2000–2017 more precipitation is observed over the western African coast and the north-eastern part of Brazil as well as north of the equator pointing to a northward shift

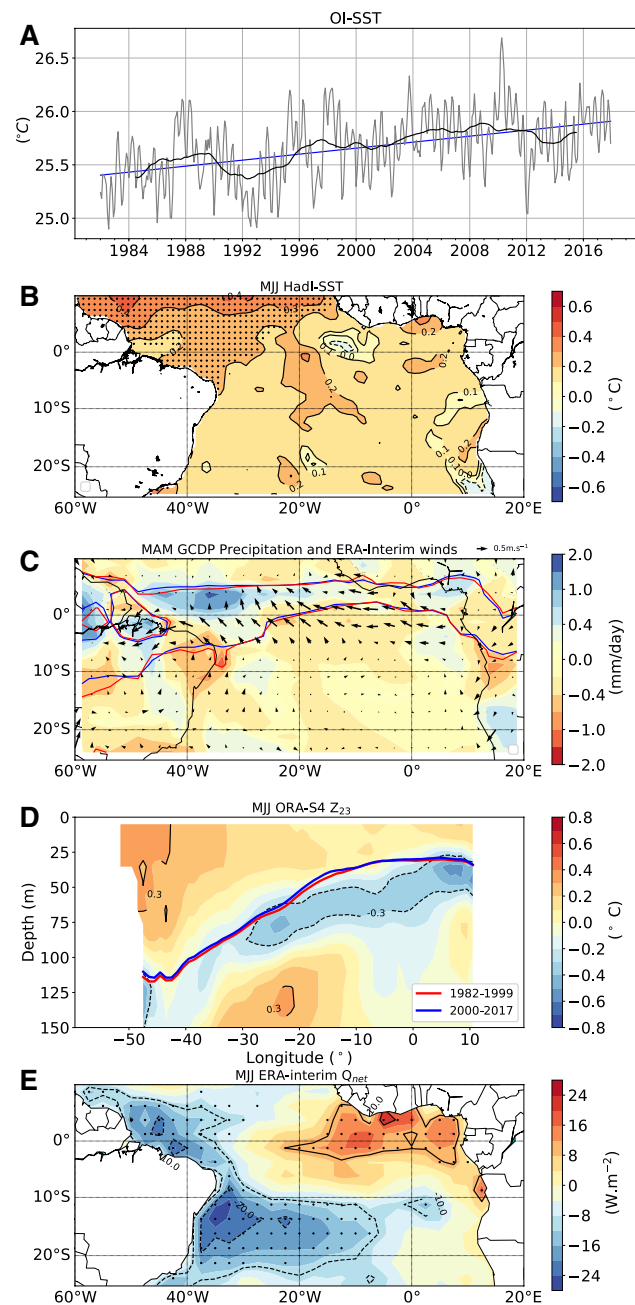


**Fig. 5** a Time series of OI-SST averaged over the tropical Atlantic basin (20° S–30° N, 60° W–15° E; gray) the 10 year running mean of SST (black) and the linear trend of SST (blue). Difference between 2000–2017 minus 1982–1999 of b MJJ HadI-SST, c MAM GPCP precipitation (shading) and ERA-Interim wind speed (shading) as well as the 5 and 10 mm day<sup>-1</sup> precipitation contours as a proxy for the ITCZ position in 1982–1999 (red) and 2000–2017 (blue), d MJJ ORA-S4 subsurface temperature superimposed by the 23 °C isotherm depth as a proxy for thermocline depth during 1982–1999 (red) and 2000–2017 (blue). e MJJ ERA-interim net heat flux. Dots indicate that the means are significantly different at 95%-level according to the Welch's t test



of the ITCZ position. The shift of the ITCZ might explain the reduced WAtl wind variability (Zebiak 1986; Richter et al. 2017). Regarding the winds, a minor intensification of the easterlies is noted over the eastern equatorial Atlantic, which is consistent with a slight shoaling of the thermocline along the equator (Fig. 5d). The changes in precipitation and wind are not significant and therefore not further discussed. A cooling of  $0.3^{\circ}\text{C}$  of the MJJ ocean temperature from  $30^{\circ}\text{W}$  to  $10^{\circ}\text{E}$  below the thermocline is observed which acts to sharpen the vertical gradient of ocean temperature along the thermocline (Fig. 5d). Compared to 1982–1999, since 2000 a stronger MJJ net heat flux is observed in the eastern equatorial Atlantic and lower in the western equatorial Atlantic. Although the eastern part of the basin receives more heat no significant warming is observed in MJJ. We hypothesize that the increased easterlies may have enhanced the upwelling along the equator and balance the heat surplus. Changes in the Walker circulation are represented by the zonal streamfunction (see Sect. 2 and Eq. 10) in Fig. 6. Compared to 1982–1999, since 2000 a strengthening and a minor westward shift of the rising branch of the Walker circulation is observed, so that it is situated slightly more over land (Fig. 6). This can also explain the reduced zonal wind variability in the western equatorial Atlantic and weakened Bjerknes feedback by a similar mechanism that was found in the Pacific: a strengthened and more westward Walker circulation weakens the wind–SST feedback and Bjerknes feedback as this hooks the rising branch of the Walker Circulation over land and therefore hampers the ocean–atmosphere coupling (Bayr et al. 2018, 2019). For the equatorial Pacific, Li et al. (2019) observed a profound shift of the Walker circulation when comparing the periods 1979–1999 and 2000–2017. This westward shift resulted in a significant change of the equatorial Pacific climate variability.

The aforementioned changes in the mean state are hardly significant and can likely not fully explain the weakening of the Bjerknes feedback. Hu et al. (2013), carrying out experiments with the Zebiak–Cane model in the tropical Pacific, found a nonlinear response of ENSO amplitudes to thermocline slope. They found that a too large thermocline slope would hinder warm water zonal migration which is unfavourable for ENSO growth. In our case, however, the larger thermocline tilt as well as the increased zonal winds explain too little variance to account for the 31% reduction of the SST variability.

We conclude that the weakening of the Bjerknes feedback fits to the changes of the background mean state and the reduced zonal wind response to SST anomalies as well as the decreased response of the ocean thermocline slope to wind stress anomalies and thus likely contributed to the reduced SST variability after 2000. We also note here that the enhanced sensitivity of the near-surface humidity difference to SSTa and slightly stronger trade winds along with warmer SSTs may have played a role in enhancing the net heat flux damping through the turbulent heat fluxes.

### 3.5 Verification using the simplest recharge oscillator

The linear recharge oscillator (ReOsc) from Burgers et al. (2005) (see Sect. 2) is a tool to diagnose ENSO-like dynamics and used here to corroborate the link between reduced SST variability, weakened Bjerknes feedback and stronger net heat flux damping during 2000–2017.

Multiple studies have shown that the simple ReOsc model is able to reproduce fundamental aspects of ENSO in the tropical Pacific (Wengel et al. 2018; Vijayeta and Dommenget 2018) and also the Bjerknes feedback and delayed negative feedback in the tropical Atlantic (Jansen et al. 2009)

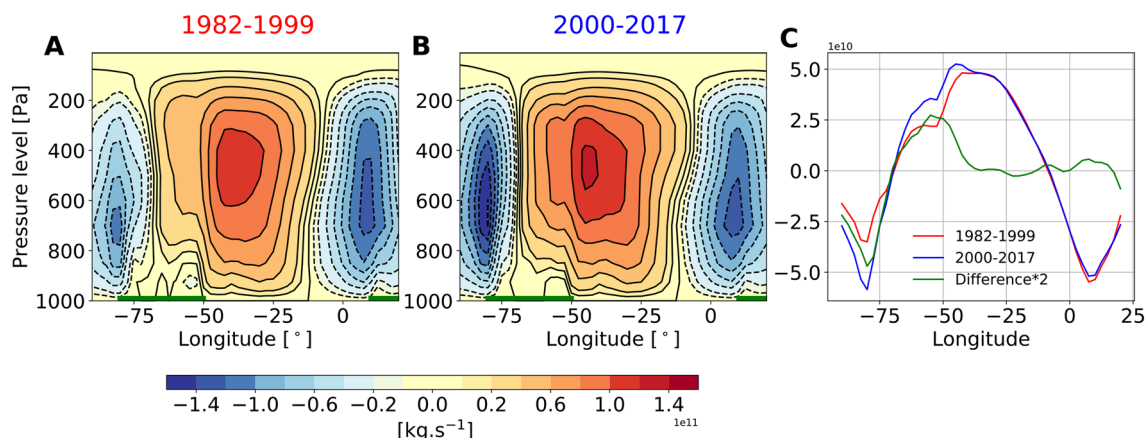


**Fig. 6** **a, b** Zonal ERA-interim streamfunctions representing the Walker circulation computed for the time periods 1982–1999 and 2000–2017, respectively. **c** Vertically integrated zonal streamfunction. Green bold lines at the bottom indicate South America and Africa

with the advantage to allow for a decomposition of the ocean and atmosphere contributions to the SST variability. The ReOsc model, however, has limitations, as it does not consider, for example, nonlinearities. Although the equatorial Atlantic variability is overestimated, mainly because of the absence of nonlinearities, the ReOsc model produces a weakening of 50% of the MJJ SST variability from 0.93 during 1982–1999 to 0.46 during 2000–2017 which overestimates but fits to the 31% reduction found with the observations and reanalysis. We consider the tendency equation of Atl3 SSTa ( $T$  in Eq. 6) and its different components are computed for the two time periods and summarized in Table 5.

Consistent with the above results, the ReOsc model displays a stronger damping of  $T$ , which changes from  $-0.27 \text{ month}^{-1}$  to  $-0.46 \text{ month}^{-1}$  from 1982–1999 to 2000–2017. Further, the term  $a_{12}$ , representing the coupling of SSTa to the thermocline depth, has experienced a strong reduction, from  $0.057$  to  $0.011 \text{ K m}^{-1} \text{ month}^{-1}$ , noting that the coupling terms are of minor importance for the strength of SST variability as shown for the Pacific (Wengel et al. 2018). Regarding the stochastic noise forcing of  $T$ ,  $\varepsilon_T$ , a significant decrease is noted from  $0.50 \text{ K month}^{-1}$  during 1982–1999 to  $0.39 \text{ K month}^{-1}$  during 2000–2017. This reduction of the stochastic noise forcing is important as Wengel et al. (2018) showed for the Pacific that it can control ENSO amplitude.

In order to disentangle the dynamics behind the stronger damping of  $T$ , and using the methodology of Vijayeta and Dommenges (2018) and Dommenges and Vijayeta (2019) that has been applied to the Pacific, the growth rate  $a_{11}$  is further decomposed into its oceanic ( $a_{11O}$ ) and atmospheric ( $a_{11A}$ ) part (see Eq. 8 for more details on the separation method).

**Table 5** ReOsc model components of the tendency equation for the MJJ Atl3 SSTa ( $T$ ) during 1982–1999 and 2000–2017

Period	$a_{11}$ (1/month)	$a_{12}$ (K/m/month)	$\varepsilon_T$ (K/month)
1982–1999	−0.271	0.0574	0.501
2000–2017	−0.456	0.0105	0.385

ORA-S4 was used for  $T$  and  $h$ , ERA-interim for the wind stress and OAflux for the net heat flux

Table 6 summarizes the results of the decomposition. During 1982–1999, the dominant growth rate factor amounting to  $1.421 \text{ month}^{-1}$  is  $a_{11\text{wind}}$  which is composed of the coupling of SSTa to local thermocline depth and of the zonal wind to SSTa (Eq. 9). The negative feedback,  $a_{11\text{HF}}$ , which represents the thermal damping, is rather weak  $-0.196 \text{ month}^{-1}$ . The combined atmospheric feedback  $a_{11A}$  on  $T$  is positive and amounts to  $1.224 \text{ month}^{-1}$ . In contrast, during 2000–2017, a much weaker atmospheric growth rate is observed with a value of  $-0.246 \text{ month}^{-1}$ .

This strong reduction is the result of two changes: first, a reduction in  $a_{11\text{wind}}$  component,  $0.204 \text{ month}^{-1}$ , which is due to a combination of the weakened zonal wind response to SSTa ( $C_{\tau T}$ ) and reduced SST-thermocline coupling ( $a_{12}$ ). The weakened zonal wind sensitivity to SSTa might be related to the slight northward shift of the ITCZ (Fig. 5c) while the reduced SST-thermocline coupling may be the result of the enhanced vertical gradient of ocean temperature (Fig. 5d). Second, the stronger thermal damping which has changed from  $-9.612 \text{ W m}^{-2} \text{ K}^{-1}$  during 1982–1999 to  $-22.03 \text{ W m}^{-2} \text{ K}^{-1}$  during 2000–2017. The  $a_{11O}$  term becomes less negative from 1982–1999 to 2000–2017, which indicates weaker damping from oceanic processes such as mean currents and would lead to an increase in SST variability. However, this effect is overcompensated by the changes of the atmospheric damping. We therefore conclude that atmospheric processes are dominant in driving the variability weakening during these time periods.

## 4 Summary and discussion

Observational and reanalysis data as well as the linear recharge oscillator model, ReOsc, were used to investigate the multidecadal reduction in interannual MJJ SST variability in the equatorial Atlantic which has considerably weakened from 1982–1999 to 2000–2017. Understanding Equatorial Atlantic SST variability is of great importance as it influences climate over the African and American continents and contribute to the variability in the Pacific and Indian Oceans (Lübbecke et al. 2018). The major feedbacks determining the MJJ SST anomalies (SSTa) in the equatorial Atlantic have been estimated to obtain insight into the

**Table 6** ReOsc model components of the tendency equation for the Atl3 MJJ SSTa ( $T$ ) during 1982–1999 and 2000–2017, in which the growth rate of  $T$ ,  $a_{11}$ , has been decomposed into its atmospheric and oceanic part

Period	$a_{11O}$	$a_{11A}$	$a_{11\text{HF}}$	$a_{11\text{wind}}$	$C_{\tau T}$	$C_{\tau T}$
1982–1999	−1.495	1.224	−0.196	1.421	−9.612	0.012
2000–2017	−0.210	−0.246	−0.450	0.204	−22.03	0.009

ORA-S4 was used for  $T$  and  $h$ , ERA-interim for the wind stress and OAflux for the net heat flux. The units are  $\text{month}^{-1}$  for the  $a$  components,  $\text{W m}^{-2} \text{ K}^{-1}$  for  $C_{\tau T}$  and  $\text{N m}^{-2} \text{ K}^{-1}$  for  $C_{\tau T}$

dynamics underlying the reduction in equatorial Atlantic interannual SST variability. First, we analyzed the positive Bjerknes feedback. The western equatorial Atlantic zonal wind stress response to eastern equatorial Atlantic SSTa has reduced during the latter period, and this reduction might be at least partly linked to the slight northward shift of the ITCZ position observed when comparing the mean boreal spring situations of 1982–1999 and 2000–2017. A northward shift of the mean deep convection could lead to a reduced wind sensitivity to SSTa (Zebiak 1986; Richter et al. 2017). Similarly, the thermocline response to western zonal wind stress anomalies has weakened during boreal summer. The surface–subsurface coupling did not exhibit a significant change.

Overall, the Bjerknes feedback weakened but the weakening cannot be fully attributed to the mean state changes which are rather weak. We did not find significant changes in the mean thermocline depth and zonal wind as found by Hu et al. (2013) for the Pacific, where a stronger thermocline tilt consistent with stronger trade winds and enhanced Walker circulation was observed after the year 2000 explaining the weakened variability on the equatorial Pacific Ocean. A cooling of the subsurface ocean temperature is found between 30° W and 10° E which enhances the vertical gradient of temperature and may help to reduce the surface–subsurface coupling. The mean tropical Atlantic MJJ SST underwent a significant warming of 0.2–0.3 K north of the equator but not much on the equator.

Second, we analyzed the net heat flux damping, the dominant negative feedback on SSTa over the equatorial Atlantic (Lübbecke and McPhaden 2013). The net heat flux damping has strongly increased during 2000–2017, which is mostly due to the stronger latent heat flux response to SSTa and found to be the result of a larger response of the air–surface specific humidity difference response to SSTa.

The linear recharge oscillator (ReOsc) allowed us to linearly decompose the ocean and atmosphere contributions to the SST variability. The results of the ReOsc show that the weakened SST variability in the eastern equatorial Atlantic is mainly due to a stronger atmosphere damping after 2000. Changes in oceanic damping are overcompensated by atmospheric processes. Besides, the MJJ stochastic forcing of the SSTa has also reduced since 2000, which might influence the amplitude of the Atlantic zonal mode as Wengel et al. (2018) showed that the stochastic forcing has an impact on ENSO amplitude. However, studying the link between the stochastic forcing and the SST variability in the equatorial Atlantic would need further research. The possibility to decompose the stochastic forcing into a state-dependent and state-independent part is noted (Levine et al. 2016), which is however beyond the scope of this paper.

Tokina and Xie (2011) studied the weakening of the equatorial Atlantic cold tongue during 1950–2009. Using

the 20 °C isotherm for the thermocline depth, they found a deepening trend of the thermocline along with a relaxation of the equatorial trade winds in the eastern Atlantic and a basin-wide warming with a local maximum in the cold tongue region. They concluded that these mean state changes together with enhanced atmospheric convection were responsible for the reduced SST variability in the equatorial Atlantic. As shown by Castaño-Tierno et al. (2018), the use of the 20 °C isotherm as a proxy for thermocline depth might impact the assessment of the air–sea coupling as the 20 °C isotherm is too deep and therefore less sensitive to changes in surface temperatures and winds. Our study shows no significant change in the trade winds, during the analysis period, or at least no weakening, which is consistent with the findings of Servain et al. (2014). The different wind trends found in different studies, depending on the exact region, time period and wind product, highlights the multidecadal variability as well as the uncertainty of wind datasets. It is known that reanalysis datasets have large biases in the tropical Atlantic (Huang et al. 2007) that may overshadow the mean state changes from one period to the other and increase the uncertainty on the ocean–atmosphere feedbacks (Kumar and Hu 2012). However, the use of several datasets allows to show the robustness of our results.

Other possible sources for multidecadal changes in the equatorial Atlantic interannual variability can be of remote origin. The El Niño/Southern Oscillation (ENSO), the dominant mode of interannual variability in the Pacific Ocean, is suggested to influence Atlantic variability in various ways (Latif and Grötzner 2000; Chang et al. 2006). Similarly to the equatorial Atlantic, the equatorial Pacific also has experienced a weakening in variability during the last 2 decades (Hu et al. 2013, 2017; Li et al. 2019), raising the question whether the two phenomena are connected. The connection between ENSO and the Atlantic Niño mode is, however, complicated (see Cai et al. (2019) for a review) and directed both from the Pacific to the Atlantic (Enfield and Mayer 1997; Latif and Grötzner 2000; Chang et al. 2006; Lübbecke and McPhaden 2013) and from the Atlantic to the Pacific (Jansen et al. 2009; Rodríguez-Fonseca et al. 2009; Ding et al. 2012). Wang (2017) showed a weakened interannual variability in the contrast in rainfall between the eastern equatorial Pacific and equatorial Atlantic since 2000. This weakening was associated with the weakened interannual variability in the inter-Pacific–Atlantic zonal SST gradient and in the associated equatorial cross-South American wind linking the two ocean basins since 2000. This study shows the importance of the influences from the Pacific on the variability of the equatorial Atlantic via Pacific–Atlantic interactions. Hence, the relationship between the weakened variability in both the equatorial Atlantic and Pacific around the year 2000 will need to be investigated further.

Finally, the Atlantic Multidecadal Oscillation (AMO) might have also played a role in the SST variability change in the equatorial Atlantic. Recently, Martín-Rey et al. (2018) showed that during a negative phase of the AMO, the equatorial Atlantic SST variability is enhanced by more than 150% in boreal summer. Wang and Zhang (2013) showed that the warm phase of AMO corresponds to a strengthening of the Atlantic meridional overturning circulation (AMOC) while Svendsen et al. (2014) showed that a weakening of the AMOC could enhance the equatorial Atlantic variability. Hence a positive phase of the AMO might tend to weaken the equatorial Atlantic variability. In the early 1990s, the AMO changed phase from negative to positive, which could have contributed to the relative weakening of the equatorial Atlantic SST variability.

**Acknowledgements** The authors would like to thank the anonymous reviewers for their constructive comments. This study was supported by the German Federal Ministry of Education and Research as part of the BANINO project (03F0795A) and the SFB 754 “Climate-Biochemistry Interactions in the tropical Ocean”. We acknowledge : the NOAA/OAR/ESRL PSD, Boulder, Colorado, USA, for providing NOAA High Resolution SST data and NCEP Reanalysis data, from their Web site at <https://www.esrl.noaa.gov/psd/>; the UK Met Office and ECMWF for providing datasets; the global ocean heat flux and evaporation products were provided by the WHOI OaFlux project (<http://oafux.whoi.edu>) funded by the NOAA Climate Observations and Monitoring (COM) program; the Climate Data Guide: GPCP (Monthly): Global Precipitation Climatology Project. Retrieved from <https://climatedataguide.ucar.edu/climate-data/gpcp-monthly-global-precipitation-climatology-project>.

## References

- Adler RF, Sapiano MR, Huffman GJ, Wang JJ, Gu G, Bolvin D, Chiu L, Schneider U, Becker A, Nelkin E, Xie P, Ferraro R, Shin DB (2018) The Global Precipitation Climatology Project (GPCP) monthly analysis (New Version 2.3) and a review of 2017 global precipitation. *Atmosphere*. <https://doi.org/10.3390/atmos9040138>
- Balmaseda MA, Mogensén K, Weaver AT (2013) Evaluation of the ECMWF ocean reanalysis system ORAS4. *Q J R Meteorol Soc* 139(674):1132–1161. <https://doi.org/10.1002/qj.2063>
- Bayr T, Dommengat D, Martin T, Power SB (2014) The eastward shift of the Walker Circulation in response to global warming and its relationship to ENSO variability. *Climate Dyn* 43(910):2747–2763. <https://doi.org/10.1007/s00382-014-2091-y>
- Bayr T, Latif M, Dommengat D, Wengel C, Harlaß J, Park W (2018) Mean-state dependence of ENSO atmospheric feedbacks in climate models. *Climate Dyn* 50(9–10):3171–3194. <https://doi.org/10.1007/s00382-017-3799-2>
- Bayr T, Wengel C, Latif M, Dommengat D, Lübbecke J, Park W (2019) Error compensation of ENSO atmospheric feedbacks in climate models and its influence on simulated ENSO dynamics. *Climate Dyn* 53(1):155–172. <https://doi.org/10.1007/s00382018-4575-7>
- Bentamy A, Katsaros KB, Mestas-Nunez AM, Drennan WM, Forde EB, Roquet H (2003) Satellite estimates of wind speed and latent heat flux over the global oceans. *J Climate* 16(4):637–656. [https://doi.org/10.1175/15200442\(2003\)016%3c0637:seowsa%3e2.0.co;2](https://doi.org/10.1175/15200442(2003)016%3c0637:seowsa%3e2.0.co;2)
- Bentamy A, Piollé JF, Grouazel A, Danielson R, Gulev S, Paul F, Azelmat H, Mathieu PP, von Schuckmann K, Sathyendranath S, Evers-King H, Esau I, Johannessen JA, Clayson CA, Pinker RT, Grodsky SA, Bourassa M, Smith SR, Haines K, Valdivieso M, Merchant CJ, Chapron B, Anderson A, Hollmann R, Josey SA (2017) Review and assessment of latent and sensible heat flux accuracy over the global oceans. *Remote Sens Environ* 201(November):196–218. <https://doi.org/10.1016/j.rse.2017.08.016>
- Bjerknes J (1969) Atmospheric teleconnections from the equatorial Pacific. *Mon Weather Rev* 97(3):163–172. [https://doi.org/10.1175/1520-0493\(1969\)097%3c0163:atftep%3e2.3.co;2](https://doi.org/10.1175/1520-0493(1969)097%3c0163:atftep%3e2.3.co;2). <https://docs.lib.noaa.gov/rescue/mwr/097/mwr-097-03-0163.pdf>
- Burgers G, Jin FF, van Oldenborgh GJ (2005) The simplest ENSO recharge oscillator. *Geophys Res Lett* 32(13):1–4. <https://doi.org/10.1029/2005gl022951>
- Cai W, Wu L, Lengaigne M, Li T, McGregor S, Kug JS, Yu JY, Stuecker MF, Santoso A, Li X, Ham YG, Chikamoto Y, Ng B, McPhaden MJ, Du Y, Dommengat D, Jia F, Kajtar JB, Keenlyside N, Lin X, Luo JJ, Martín-Rey M, Ruprich-Robert Y, Wang G, Xie SP, Yang Y, Kang SM, Choi JY, Gan B, Kim GI, Kim CE, Kim S, Kim JH, Chang P (2019) Pan-tropical climate interactions. *Science*. <https://doi.org/10.1126/science.aav4236>
- Castaño-Tierno A, Mohino E, Rodríguez-Fonseca B, Losada T (2018) Revisiting the CMIP5 thermocline in the equatorial Pacific and Atlantic Oceans. *Geophys Res Lett* 45:12,963–12,971. <https://doi.org/10.1029/2018GL079847>
- Chang P, Fang Y, Saravanan R, Ji L, Seidel H (2006) The cause of the fragile relationship between the Pacific El Niño and the Atlantic Niño. *Nature* 443(7109):324–328. <https://doi.org/10.1038/nature05053>
- Dee DP, Uppala SM, Simmons AJ, Berrisford P, Poli P, Kobayashi S, Andrae U, Balmaseda MA, Balsamo G, Bauer P, Bechtold P, Beljaars AC, van de Berg L, Bidlot J, Bormann N, Delsol C, Dragani R, Fuentes M, Geer AJ, Haimberger L, Healy SB, Hersbach H, Hólm EV, Isaksen I, Kallberg P, Köhler M, Matricardi M, McNally AP, Monge-Sanz BM, Morcrette JJ, Park BK, Peubey C, de Rosnay P, Tavolato C, Thépaut JN, Vitart F (2011) The ERA-Interim reanalysis: configuration and performance of the data assimilation system. *Q J R Meteorol Soc* 137(656):553–597. <https://doi.org/10.1002/qj.828>
- Deppenmeier AL, Haarsma RJ, Hazeleger W (2016) The Bjerknes feedback in the tropical Atlantic in CMIP5 models. *Climate Dyn* 47(7–8):2691–2707. <https://doi.org/10.1007/s00382-016-2992-z>
- Ding H, Keenlyside NS, Latif M (2012) Impact of the Equatorial Atlantic on the El Niño Southern Oscillation. *Climate Dyn* 38(9–10):1965–1972. <https://doi.org/10.1007/s00382-011-1097-y>
- Dippe T, Lübbecke JF, Greatbatch RJ (2019) A comparison of the Atlantic and Pacific Bjerknes feedbacks: seasonality, symmetry, and stationarity. *J Geophys Res Oceans* 124(4):2374–2403. <https://doi.org/10.1029/2018jc014700>
- Dommengat D, Vijayeta A (2019) Simulated future changes in ENSO dynamics in the framework of the linear recharge oscillator model. *Climate Dyn*. <https://doi.org/10.1007/s00382-019-04780-7>
- Enfield DB, Mayer DA (1997) Tropical Atlantic sea surface temperature variability and its relation to El Niño-Southern Oscillation. *J Geophys Res* 102:929–945
- Folland CK, Palmer TN, Parker DE (1986) Sahel rainfall and worldwide sea temperatures, 1901–85. *Nature* 320(6063):602–607. <https://doi.org/10.1038/320602a0>
- Frankignoul C, Kestenare E, Mignot J (2002) The surface heat flux feedback. Part II: direct and indirect estimates in the ECHAM4/OPA8 coupled GCM. *Climate Dyn* 19(8):649–656. <https://doi.org/10.1007/s00382-002-0253-9>



- Frauen C, Dommenges D (2010) El Niño and la Niña amplitude asymmetry caused by atmospheric feedbacks. *Geophys Res Lett* 37(18):1–6. <https://doi.org/10.1029/2010gl044444>
- Guan C, McPhaden MJ (2016) Ocean processes affecting the Twenty-First-Century shift in ENSO SST variability. *J Climate* 29(19):6861–6879. <https://doi.org/10.1175/jcli-d-15-0870.1>
- Harlaß J, Latif M, Park W (2015) Improving climate model simulation of tropical Atlantic sea surface temperature: the importance of enhanced vertical atmosphere model resolution. *Geophys Res Lett* 42:2401–2408. <https://doi.org/10.1002/2015gl063310>
- Hersbach H, Dee D (2016) ERA5 reanalysis is in production. *ECMWF Newsl* 147:7
- Hirst Antrony C, Hastenrath S (1983) Atmosphere-ocean mechanisms of climate anomalies in the Angola-Tropical Atlantic sector. *J Phys Oceanogr* 13(7):1146–1157. [https://doi.org/10.1175/1520-0485\(1983\)013%3c1146:aomoca%3e2.0.co;2](https://doi.org/10.1175/1520-0485(1983)013%3c1146:aomoca%3e2.0.co;2)
- Hu ZZ, Kumar A, Ren HL, Wang H, L'heureux M, Jin FF (2013) Weakened interannual variability in the Tropical Pacific Ocean since 2000. *J Climate* 26(8):2601–2613. <https://doi.org/10.1175/jcli-d-12-00265.1>
- Hu Z-Z, Kumar A, Huang B et al (2017) Interdecadal variations of ENSO around 1999/2000. *J Meteorol Res* 31(1):73–81. <https://doi.org/10.1007/s13351-017-6074-x>
- Huang B et al (2007) Evolution of model systematic errors in the tropical Atlantic basin from the NCEP coupled hindcasts. *Climate Dyn* 28(7–8):661–682. <https://doi.org/10.1007/s00382-006-0223-8>
- Jansen MF, Dommenges D, Keenlyside N (2009) Tropical atmosphere—ocean interactions in a conceptual framework. *J Climate* 22(3):550–567. <https://doi.org/10.1175/2008jcli2243.1>
- Jin F-F, Kim ST, Bejarano L (2006) A coupled-stability index for ENSO. *Geophys Res Lett* 33:2–5. <https://doi.org/10.1029/2006gl027221>
- Jouanno J, Hernandez O, Sanchez-Gomez E (2017) Equatorial Atlantic interannual variability and its relation to dynamic and thermodynamic processes. *Earth Syst Dyn* 8(4):1061–1069. <https://doi.org/10.5194/esd-8-1061-2017>
- Kalnay E, Kanamitsu M, Kistler R, Collins W, Deaven D, Gandin L, Iredell M, Saha S, White G, Woollen J, Zhu Y, Chelliah M, Ebisuzaki W, Higgins W, Janowiak J, Mo KC, Ropelewski C, Wang J, Leetmaa A, Reynolds R, Jenne R, Joseph D (1996) The NCEP/NCAR 40-year reanalysis project. *Bull Am Meteorol Soc* 77:437–472. [https://doi.org/10.1175/1520-0477\(1996\)077%3c0437:TNYRP%3e2.0.CO;2](https://doi.org/10.1175/1520-0477(1996)077%3c0437:TNYRP%3e2.0.CO;2)
- Kanamitsu M, Ebisuzaki W, Woollen J, Yang S, Hnilo JJ, Fiorino M, Potter GL (2002) NCEP–DOE AMIP-II reanalysis (R-2). *Bull Am Meteorol Soc* 83:1631–1644. <https://doi.org/10.1175/BAMS-83-11-1631>
- Keenlyside NS, Latif M (2007) Understanding equatorial Atlantic interannual variability. *J Climate* 20(1):131–142. <https://doi.org/10.1175/jcli3992.1>
- Kumar A, Hu Z-Z (2012) Uncertainty in the ocean-atmosphere feedbacks associated with ENSO in the reanalysis products. *Climate Dyn* 39(3–4):575–588. <https://doi.org/10.1007/s00382-011-1104-3>
- Latif M, Grötzner A (2000) The equatorial Atlantic oscillation and its response to ENSO. *Climate Dyn* 16(2–3):213–218. <https://doi.org/10.1007/s003820050014>
- Levine A, Jin F-F, McPhaden MJ (2016) Extreme noise-extreme El Niño: how state-dependent noise forcing creates El Niño–La Niña asymmetry. *J Climate* 29:5483–5499. <https://doi.org/10.1175/jcli-d-16-0091.1>
- Li X et al (2019) On the westward shift of tropical Pacific climate variability since 2000. *Climate Dyn*. <https://doi.org/10.1007/s00382-019-04666-8>
- Lloyd J, Guilyardi E, Weller H (2011) The role of atmosphere feedbacks during ENSO in the CMIP3 models. Part II: using AMIP runs to understand the heat flux feedback mechanisms. *Climate Dyn* 37:1271–1292. <https://doi.org/10.1175/jcli-d-11-00178.1>
- Lübbecke Joke F, McPhaden MJ (2013) A comparative stability analysis of Atlantic and Pacific Niño mode. *J Climate* 26(16):5965–5980. <https://doi.org/10.1175/jcli-d-12-00758.1>
- Lübbecke JF, McPhaden MJ (2014) Assessing the twenty-first-century shift in ENSO variability in terms of the Bjerknes Stability Index. *J Climate* 27:2577–2587. <https://doi.org/10.1175/jcli-d-13-00438.1>
- Lübbecke JF, McPhaden MJ (2017) Symmetry of the Atlantic Niño mode. *Geophys Res Lett* 44(2):965–973. <https://doi.org/10.1002/2016gl071829>
- Lübbecke JF, Rodríguez-Fonseca B, Richter I, Martín-Rey M, Losada T, Polo I, Keenlyside NS (2018) Equatorial Atlantic variability—modes, mechanisms, and global teleconnections. *Wiley Interdiscip Rev Climate Change* 9(4):1–18. <https://doi.org/10.1002/wcc.527>
- Martín-Rey M, Polo I, Rodríguez-Fonseca B, Losada T, Lazar A (2018) Is there evidence of changes in Tropical Atlantic variability modes under AMO phases in the observational record? *J Climate* 31:515–536. <https://doi.org/10.1175/JCLI-D-16-0459.1>
- Namchi HC, Li J, Kucharski F, Kang IS, Keenlyside NS, Chang P, Farneti R (2015) Thermodynamic controls of the Atlantic Niño. *Nat Commun*. <https://doi.org/10.1038/ncomms9895>
- Nobre P, Shukla J (1996) Variations of SST, wind stress and rainfall over the tropical Atlantic and South America. *J Climate* 9(May):2464–2479. [https://doi.org/10.1175/1520-0442\(1996\)009%3c2464](https://doi.org/10.1175/1520-0442(1996)009%3c2464)
- Okumura Y, Xie SP (2006) Some overlooked features of tropical Atlantic climate leading to a new Niño-like phenomenon. *J Climate* 19(22):5859–5874. <https://doi.org/10.1175/jcli3928.1>
- Rayner NA (2003) Global analyses of sea surface temperature, sea ice, and night marine air temperature since the late nineteenth century. *J Geophys Res* 108(D14):4407. <https://doi.org/10.1029/2002jd002670>
- Reynolds RW, Smith TM, Liu C, Chelton DB, Casey KS, Schlax MG (2007) Daily high-resolution-blended analyses for sea surface temperature. *J Climate* 20:5473–5496. <https://doi.org/10.1175/2007JCLI1824.1>
- Richter I, Xie SP, Morioka Y, Doi T, Taguchi B, Behera S (2017) Phase locking of equatorial Atlantic variability through the seasonal migration of the ITCZ. *Climate Dyn* 48(11–12):3615–3629. <https://doi.org/10.1007/s00382-016-3289-y>
- Rodríguez-Fonseca B, Polo I, García-Serrano J, Losada T, Mohino E, Mechoso CR, Kucharski F (2009) Are Atlantic Niños enhancing Pacific ENSO events in recent decades? *Geophys Res Lett*. <https://doi.org/10.1029/2009gl040048>
- Saha S, Moorthi S, Wu X, Wang J, Nadiga S, Tripp P, Behringer D, Hou Y, Chuang H, Iredell M, Ek M, Meng J, Yang R, Mendez MP, van den Dool H, Zhang Q, Wang W, Chen M, Becker E (2014) The NCEP climate forecast system version 2. *J Climate* 27:2185–2208. <https://doi.org/10.1175/JCLI-D-12-00823.1>
- Servain J, Picaut J, Merle J (1982) Evidence of remote forcing in the Equatorial Atlantic Ocean. *J Phys Oceanogr*. [https://doi.org/10.1175/1520-0485\(1982\)012%3c0457:eorfit%3e2.0.co;2](https://doi.org/10.1175/1520-0485(1982)012%3c0457:eorfit%3e2.0.co;2)
- Servain J, Caniaux G, Kouadio YK, McPhaden MJ, Araujo M (2014) Recent climatic trends in the tropical Atlantic. *Climate Dyn* 43(11):3071–3089. <https://doi.org/10.1007/s00382-014-2168-7>
- Svendsen L, Kvamstø N-G, Keenlyside N (2014) Weakening AMOC connects Equatorial Atlantic and Pacific interannual variability. *Climate Dyn* 43:2931–2941. <https://doi.org/10.1007/s00382-013-1904-8>
- Tokinaga H, Xie SP (2011) Weakening of the equatorial Atlantic cold tongue over the past six decades. *Nat Geosci* 4(4):222–226. <https://doi.org/10.1038/ngeo1078>
- Vijayeta A, Dommenges D (2018) An evaluation of ENSO dynamics in CMIP simulations in the framework of the recharge oscillator

- model. *Climate Dyn* 51(5):1753–1771. <https://doi.org/10.1007/s00382-017-3981-6>
- Wang L (2017) Weakened interannual variability of the contrast in rainfall between the eastern equatorial Pacific and equatorial Atlantic since 2000. *Atmos Ocean Sci Lett* 10(3):198–205. <https://doi.org/10.1080/16742834.2017.1286632>
- Wang C, Zhang L (2013) Multidecadal ocean temperature and salinity variability in the tropical North Atlantic: linking with the AMO, AMOC, and subtropical cell. *J Climate* 26:6137–6162. <https://doi.org/10.1175/JCLI-D-12-00721.1>
- Wengel C, Dommenges D, Latif M, Bayr T, Vijayeta A (2018) What controls ENSO-amplitude diversity in climate models? *Geophys Res Lett* 45(4):1989–1996. <https://doi.org/10.1002/2017gl076849>
- Xu K, Wang W, Liu B, Zhu C (2019) Weakening of the El Niño amplitude since the late 1990s and its link to decadal change in the North Pacific climate. *Int J Climatol*. <https://doi.org/10.1002/joc.6063>
- Yu L, Jin X, Weller RA (2008) Multidecade global flux datasets from the objectively analyzed air-sea fluxes (OAFlux) project: latent and sensible heat fluxes, ocean evaporation, and related surface meteorological variables. OAFlux project technical report. OA-2008-01. Woods Hole Oceanographic Institution, Woods Hole, Massachusetts
- Zebiak SE (1986) Atmospheric convergence feedback in a simple model for El Niño. *Mon Weather Rev* 114:1263–1271
- Zebiak SE (1993) Air–sea interaction in the Equatorial Atlantic Region. *J Climate* 6(8):1567–1586. [https://doi.org/10.1175/1520-0442\(1993\)006%3c1567:aiitea%3e2.0.co;2](https://doi.org/10.1175/1520-0442(1993)006%3c1567:aiitea%3e2.0.co;2)

**Publisher's Note** Springer Nature remains neutral with regard to jurisdictional claims in published maps and institutional affiliations.